Isitman, Ogulcan; Bettahar, Houari; Zhou, Quan

Non-Contact Cooperative Manipulation of Magnetic Microparticles Using Two Robotic Electromagnetic Needles

Published in:
IEEE Robotics and Automation Letters

DOI:
10.1109/LRA.2021.3137546

Published: 01/04/2022

Document Version
Publisher's PDF, also known as Version of record

Non-Contact Cooperative Manipulation of Magnetic Microparticles Using Two Robotic Electromagnetic Needles

Oğulcan Işıtman, Houari Bettahar, and Quan Zhou, *Member, IEEE*

***Abstract*—In this paper, we report a cooperative manipulation method for non-contact robotic electromagnetic needle manipulation system. We employ two 3 degrees of freedom (DOF) robotic electromagnetic needles to achieve an over-actuated manipulator, which can move the particle to any position in the planar workspace from any direction. The redundant DOFs, combined with an optimization-based control approach, enable the manipulator to achieve accurate path following and avoid the collision of needles. Using visual servoing, the developed controller can achieve line following accuracy of 0.33 ± 0.32 μm, square following accuracy of 0.77 ± 0.55 μm, and circle following accuracy of 0.89 ± 0.66 μm with a 4.5 μm diameter superparamagnetic particle. The manipulator can also manipulate a particle along complex paths such as infinity symbol and letter symbols.**

***Index Terms*—Cooperating robots, automation at micro-nano scales, micro/nano robots.**

I. Introduction

COOPERATION of multiple robotic manipulators has been an important technique to achieve tasks that are difficult or not feasible with single manipulators [1]. Such cooperative robotic manipulation systems are widely used in applications such as manufacturing of consumer products [2], [3], assembly parts in the outer space [4], rehabilitation of patients [5], and complex sample preparation in laboratory automation [6]. Many previous reported cooperative manipulators are developed to manipulate objects of size from several meters to several millimeters [3], [7]. They often rely on the rigid contact between the object and the end effectors of the manipulator. Cooperative manipulation of microscale objects has also been reported, e.g., caging micromanipulation using four cooperative contact probes [8].

Manuscript received August 17, 2021; accepted December 3, 2021. Date of publication December 23, 2021; date of current version January 14, 2022. This work was supported by the Academy of Finland under Projects 317018 and 331149. This letter was recommended for publication by Associate Editor L. Pimenta and Editor M. Hsieh upon evaluation of the reviewers' comments. (*Corresponding author: Quan Zhou.*)

The authors are with the Department of Electrical Engineering and Automation, School of Electrical Engineering, Aalto University, 00076 Aalto, Finland (e-mail: ogulcan.isitman@aalto.fi; houari.bettahar@aalto.fi; quan.zhou@aalto.fi).

This letter has supplementary downloadable material available at https://doi.org/10.1109/LRA.2021.3137546, provided by the authors.

Digital Object Identifier 10.1109/LRA.2021.3137546

Magnetic field-driven microrobotic manipulation of agents has piqued the interest of researchers, with a wide range of applications. Due to its transparency to human and animal tissues when the field is weak and varying slowly [9] and the capability to address micro-objects wirelessly, magnetic fields have been widely used in robotic micromanipulation. Magnetic-driven microrobotic systems have been demonstrated in performing independent control of multiple magnetic agents in 2D [10] and 3D [11], selective manipulation and extraction [12], [13], swarm motion and patterning [14], [15], as well as carrying out targeted gene delivery [16] and climbing on liquid menisci [17], among a plethora of other reported capabilities [10], [11] and [18]. Over the previous two decades, many impressive results have been reported, including contactless ocular operations, targeted drug delivery [7], [19] and [20] in-vitro diagnosis [21], endoscopy [22], minimally invasive operation [23], and environmental remediation [24], [25].

However, cooperative manipulation technique is hardly applied in magnetic field-driven manipulation. Magnetic field-driven manipulation is usually achieved by several stationary coils. One of the well-established technique to manipulate small-scale magnetic objects is to use three pairs of Helmholtz coils to generate rotating, oscillating, or uniform magnetic fields as demonstrated in [14], [16] and [17]. Depending on the target field distribution or object velocity or force vector, currents on different coils are calculated based on the models of the system. For example, eight coils are worked together in [11] to independently manipulation multiple geometrically or magnetically distinct microrobots in three dimensions. In [26] researchers used nine electromagnetic coils and current minimizing techniques to achieve simultaneous manipulation of two identical microspheres. In [18], researchers proposed a ferrofluidic manipulator consisting of 8 small-scale magnetic coils to manipulate 550 μm diameter spherical non-magnetic particles. Despite the advanced capabilities, most of those magnetic manipulation technologies create global magnetic fields using multiple fixed magnetic sources.

A robotic electromagnetic needle is a promising magnetic field-driven manipulation technique with a mobile magnetic source that can selectively manipulate microparticles [27], [12]. Seon *et al.* has shown automatic non-contact manipulation using an electromagnetic needle that can achieve velocity control, path following, separating two adjacent particles, selective extraction

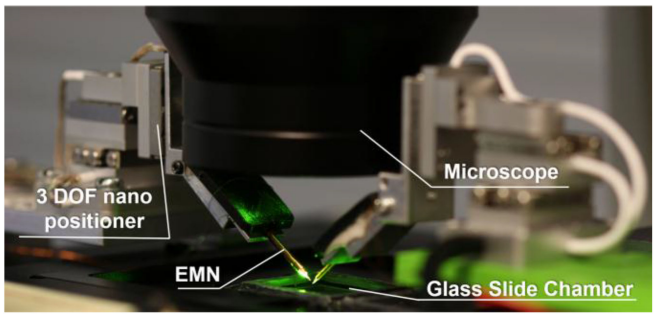

Fig. 1. Image of the two-needle robotic electromagnetic needle manipulator.

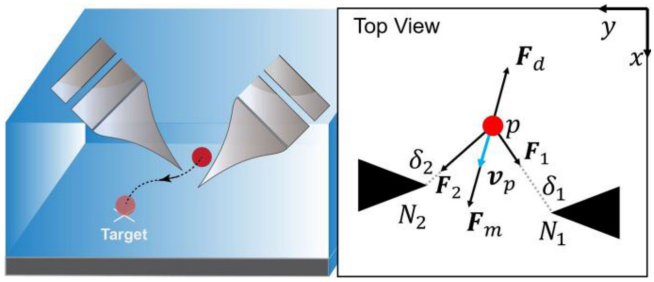

Fig. 2. Illustration of non-contact cooperative manipulation (left) and particle motion dynamics (right). The magnetic forces $\mathbf{F}_1$ and $\mathbf{F}_2$ act on the particle are pointing towards the tip each needle. The drag force $\mathbf{F}_d$ is opposite to the direction of motion of the particle, and $\mathbf{v}_p$ is the particle velocity where the direction is the same as the magnetic force $\mathbf{F}_m$. N_i is position of the tip of i^{th} needle.

of particles from a population, and independent manipulation of four particles [13]. In the work, a single needle is used to manipulate a 5 μm particle. Despite its benefits, the manipulation capability after a particle is extracted or selected is limited to the motion directed towards the needle.

In this paper, we report a cooperative manipulation method for non-contact robotic electromagnetic needle manipulation system. We employ two 3 DOF robotic electromagnetic needles to achieve an over-actuated manipulator, which can move the particle to any position in the planar workspace from any direction. The redundant DOFs, combined with an optimization-based control approach, enable the manipulator to achieve accurate path following and avoid the collision of needles. This paper is organized as follows. Section II defines the concept of the two needles cooperative micromanipulation system. Section III models the manipulation of microparticles using electromagnetic needles. Section IV describes the proposed control approach. Section V reports and discusses the obtained experimental results. Finally, Section VI concludes the paper.

II. Apparatus and Materials

To achieve cooperative non-contact micro manipulation, we use a robotic electromagnetic needle system as shown in-Fig. 1. The system consists of two electromagnetic needles, each mounted on a 3 DOF nanopositioner.

The needles are made of stainless steel, of 0.5 mm in diameter and 25 mm in length with a tip radius of around 15 μm, similar to the one used on our previous work [13]. The needles are coiled with copper wire (AWG 34) for about 300 turns in four layers. The 3 DOF nanopositioner is built from three identical stages (SLC1720, SmarACT, Germany) with sub-nanometer resolution and a maximum range of 12 mm. The microparticles are polystyrene encapsulated fluorescent iron-III-oxide (Fe3O4@PS, Microparticles Germany) with a mean diameter of 4.54 μm, density of 1.5 g/cc, mass susceptibility of $\sim 1,7 \times 10^{-4}\ m^3\ kg^{-1}$ and saturation magnetization of $\sim 16\ \mathrm{Am^2\ kg^{-1}}$ Superparamagnetic microparticles (10 μL of stock dispersion, particle concentration: %1 w/v) were diluted with 100mL of water (deionized Milli-Q). A dose of $\sim$10 μL solution yields hundreds of microparticles within the sample carrier.

A video camera (Prime BSI, Teledyne Photometrics, USA) attached to an inverted microscope (Axio Vert.A1, Zeiss, Germany) provides visual feedback. The workspace is observed with an $\times$20 dry objective (LD A-Plan 20x/0,35 Ph1 Zeiss, Germany). The camera resolution is 2048 $\times$ 2048 pixels, and the resulting field of view is about 1024 μm x 1024 μm.

A data acquisition device (NI 6343, National Instruments, USA) is used to control the electromagnetic needles, where the computer-generated signal is amplified by a current amplifier (TS200, Accel Instruments, USA). A constant current of 0.18 A is supplied to the needles unless they are turned off intentionally.

III. Concept of the Non-Contact Cooperative Manipulation

The magnetic force acting on a single particle from a needle is the negative gradient of the magnetic potential energy (U):

$$\boldsymbol{F} = -\nabla U = -\nabla\ (\boldsymbol{m}_{\mathrm{p}} \cdot \boldsymbol{B}) = -\mu_0\ \nabla\,(\boldsymbol{m}_{\mathrm{p}} \cdot \boldsymbol{H}) \quad (1)$$

where μ_0 the vacuum permeability, $\boldsymbol{m}_p$ is the magnetic moment of a single particle, $\boldsymbol{B}$ the magnetic flux density, $\boldsymbol{H}$ the magnetic field. Note, in this paper, the bold symbols represent vectors.

Assuming the size of the particle is negligible compared to particle-needle distance, the total magnetic field generated by two needles can be described as:

$$\boldsymbol{H} = \boldsymbol{H}_1 + \boldsymbol{H}_2 \quad (2)$$

where the magnetic field generated from each magnetic needle can be presented as [28]:

$$\boldsymbol{H}_i = \frac{M_n}{4\beta\delta_i + 1}\ \boldsymbol{u}_i \quad (3)$$

where M_n is the needle core magnetization, which is a function of magnetic susceptibility of the material, number of turns per unit length, and applied current to the needle, β is the pole shape coefficient, δ_i is the distance between the particle and the tip of the i^{th} needle, $\delta_i = \|N_i - p\|$, see Fig. 2. $\boldsymbol{u}_i$ represents the unit vector directing from particle to the needle. Here we treat the two needles as identical such that $M_{n1} = M_{n2} = M_n$ and $\beta_1 = \beta_2 = \beta$.

Then the magnetic field gradient can be expressed as:

$$\frac{d\boldsymbol{H}}{d\delta_i} = \frac{4\beta M_n}{(4\beta\delta_i + 1)^2}\,\boldsymbol{u}_i \tag{4}$$

The magnetic force between a particle and a needle tip can be represented as the following:

$$\boldsymbol{F}_i = -\frac{4m_p\mu_0\beta M_n}{(4\beta\delta_i + 1)^2}\boldsymbol{u}_i \tag{5}$$

where m_p is the scalar magnitude of the magnetic moment of a single particle and magnetic force $\boldsymbol{F}_m = \boldsymbol{F}_1 + \boldsymbol{F}_2$. The magnetic particles are immersed inside water and their motion is damped by the hydrodynamic drag force, $\boldsymbol{F}_d$, which can be expressed by using Stoke's law for spherical objects:

$$\boldsymbol{F}_d = -3\pi v_f d_p \boldsymbol{v}_p \tag{6}$$

where v_f is the fluid density, $\boldsymbol{v}_p$ is particle velocity and d_p is the particle diameter.

The constant voltage supplied to both coils generates a localized magnetic field and hence force that pulls the magnetic particle towards the high magnetic field created by the needles. Since the particle is heavier than water and hovering on the surface of the glass slide due to an electric double layer [29], the particle dynamics in the x-y plane can be defined as:

$$\boldsymbol{F}_d + m\,\boldsymbol{a}_p = \boldsymbol{F}_m \tag{7}$$

where $\boldsymbol{a}_p$ is the acceleration of the particle, $\boldsymbol{F}_m$ the magnetic force exerted on the particle, $\boldsymbol{F}_m = \boldsymbol{F}_1 + \boldsymbol{F}_2$. Since the particle is ∼4.5 μm in diameter, the inertia term can be neglected, and we can treat $\boldsymbol{F}_d = \boldsymbol{F}_m$. Then (7) can be rewritten as:

$$\boldsymbol{v}_p = -\frac{\boldsymbol{F}_1 + \boldsymbol{F}_2}{3\pi v_f d_p} \tag{8}$$

Substituting (5) into (8),

$$\boldsymbol{v}_p\ (\delta_1, \delta_2) = C\left(\frac{1}{(4\beta\delta_1 + 1)^2}\boldsymbol{u}_1 + \frac{1}{(4\beta\delta_2 + 1)^2}\boldsymbol{u}_2\right) \tag{9}$$

where the coefficient $C = 4\mu_0 m_p \beta M_n / 3\pi v_f d_p$.

The non-contact cooperative manipulation is illustrated in Fig. 2 with a free body diagram.

Identifying the parameters in C in (9) is not trivial since each particle has variations in size and the amount of magnetic substance. Therefore, we employed an experimentally estimated model of particle velocity $\boldsymbol{v}_m(\delta_1, \delta_2)$ as a function of particle-needle distances to develop the proposed optimization-based control approach. The details of the experimental estimations of velocity model parameters are presented in experimental section.

IV. Optimization-Based Control

The electromagnetic manipulator having two cooperative needles is an over-actuated system. To achieve unique manipulation actions that satisfy the physical constraints of the system, we formulate the system as an optimization method with constraints.

The controller aims to find the optimal needle positions that minimize the error between the modeled velocity $\boldsymbol{v}_m$ and the target velocity $\boldsymbol{v}_t$, while avoiding potential collision of the needles. Seeking a solution in the vicinity of the current needle position is important to avoid hydrodynamic disturbance to the particle and the environment due to the large displacement of the needles.

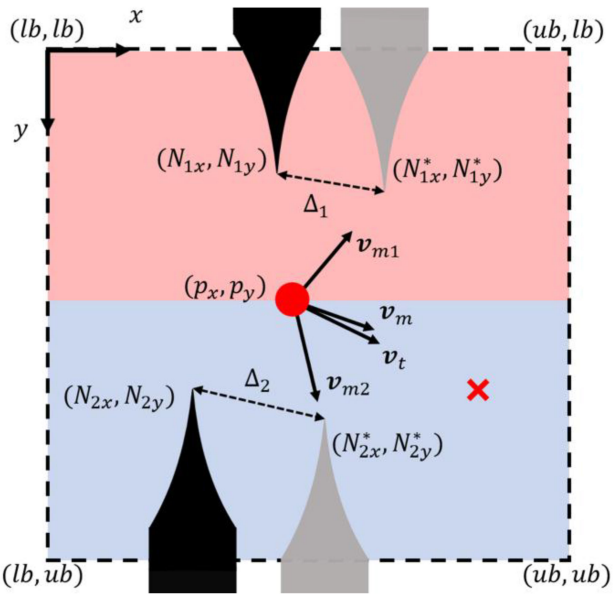

Fig. 3. Cooperative control concept. The red cross represents the target position for the particle. (p_x, p_y) is the current position of the particle (in red). $\mathbf{v}_t$, and $\mathbf{v}_m$ are the target velocity and modelled velocity, and $\mathbf{v}_{m1}$ and $\mathbf{v}_{m2}$ the particle velocity components induced by respective needle. The current needle positions (in black) are (N_{ix}, N_{iy}), the predicted optimal needle positions (in grey) are (N^*_{ix}, N^*_{iy}). The displacement between the needle positions are denoted by $\Delta N_{i=1..2}$. lb and ub are the upper and lower boundary constraints, respectively.

The cooperative manipulation scheme can be visualized in Fig. 3.

The input for the algorithm is the target particle velocity $\boldsymbol{v}_t$, the current positions of needles N_i, $N_i \in R^2$ for $i \in \{1,\ 2\}$ and the particle position, p, $p \in R^2$. The cost function J can be expressed as:

$$\underset{N_1, N_2}{\operatorname{argmin}} J = w_1\left(\|\boldsymbol{v}_t - \boldsymbol{v}_m\left(\delta_1, \delta_2\right)\|\right) + w_2\left(\Delta N_1 + \Delta N_2\right)$$

$$\text{subject to}: \begin{cases} \begin{bmatrix} lb \\ lb \\ lb \\ p_y + \in \end{bmatrix} \le \begin{bmatrix} N_{1x} \\ N_{1y} \\ N_{2x} \\ N_{2y} \end{bmatrix} \le \begin{bmatrix} ub \\ p_y - \in \\ ub \\ ub \end{bmatrix} \\ \dfrac{\|v_{mi}\left(\delta_i\right)\|}{\|v_m\left(\delta_1, \delta_2\right)\|} \ge k_c \end{cases} \tag{10}$$

where $\delta_i = \|N_i - p\|$, $\Delta N_i = \|N_i^* - N_i\|$, $N_i \in R^2$ and $\|\cdot\|$ represents the Euclidean norm of a vector. The term $\in$ is added to y-direction boundaries to provide a distance margin between the needles to avoid collision. Other variables are explained in Fig. 3.

In (10), the modeled particle velocity $\boldsymbol{v}_m$ is calculated from difference between the current needle positions $N_i = (N_{ix}, N_{iy})$, and particle position $p = (p_x, p_y)$. The first term of the cost function penalizes the error between the modeled velocity $\boldsymbol{v}_m$ and the target velocity $\boldsymbol{v}_t$. The second term is to penalize the needle displacement during manipulation to achieving small incremental needle motion that reduces hydrodynamic

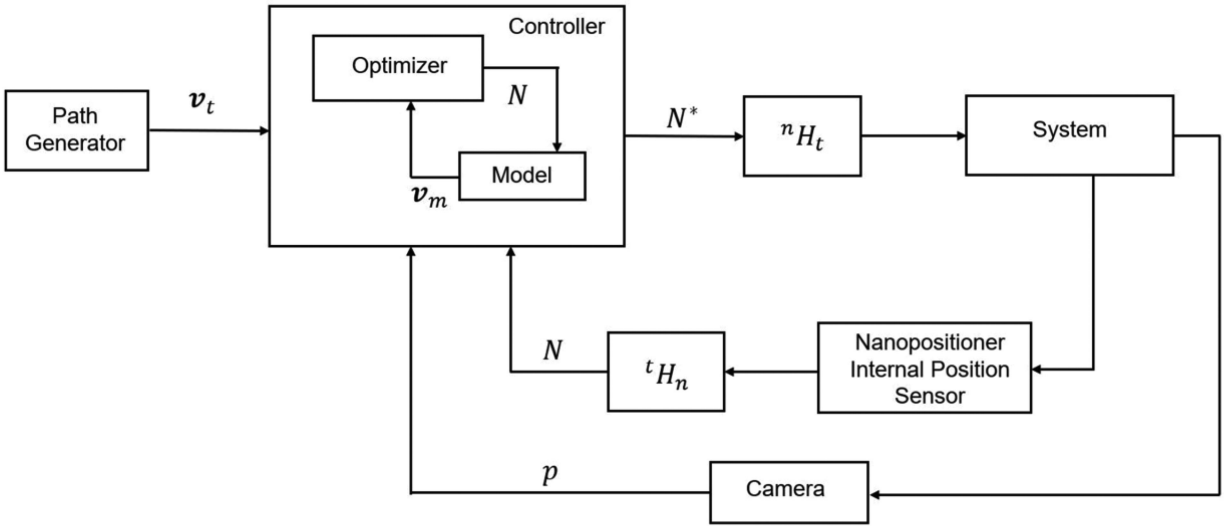

Fig. 4. Optimization-based path following control scheme for magnetic micro-particle control using two cooperative electromagnetic needles.

disturbance. w_1 and w_2 are the weights of the 1st and 2nd terms, respectively.

The algorithm returns optimal needle positions $N^* \in R^4$, where

$$N^* = \begin{bmatrix} N^*_{1x} \\ N^*_{1y} \\ N^*_{2x} \\ N^*_{2y} \end{bmatrix} \tag{11}$$

To avoid a potential collision, the motion of each needle can operate either in the upper (red) or lower (blue) half-plane separated by the particle within the boundary defined by ub and lb in (10).

In cooperative manipulation, many motions can be achieved using a single needle. However, such manipulation will cause the less active needle to be moved far away from the particle. In the case the inactive needle should participate in manipulation in the next step, a dramatic motion of the needle is often needed, which may disturb the motion of the particle. To avoid such dramatic motion, we ensure that the task is always distributed between the needles such that each needle is actively contributing to the particle motion. This is similar to the tension distribution of the cable-driven robots as the tension of all the cables must be positive [30]. In practice, we use a cooperation coefficient k_c that is the ratio between the contribution of modelled particle velocity towards any needle $\boldsymbol{v}_{mi}$ and the total modelled particle velocity $\boldsymbol{v}_m$.

The overall control scheme is shown in Fig. 4., where a controller including an optimizer and a model. The optimizer uses the cost function described above to find the optimal needle positions using the experimentally obtain velocity model $\boldsymbol{v}_m(\delta_1, \delta_2)$, explained in the Experimental Section. The controller gets the target velocities $\boldsymbol{v}_t$ from a path generator, and measurement of the particle position p from camera and needle positions N_i from internal sensors of 3 DOF nano-positioner. The output of the controller is the optimal needle positions that command the motion of the system especially the 3 DOF nanopositioner.

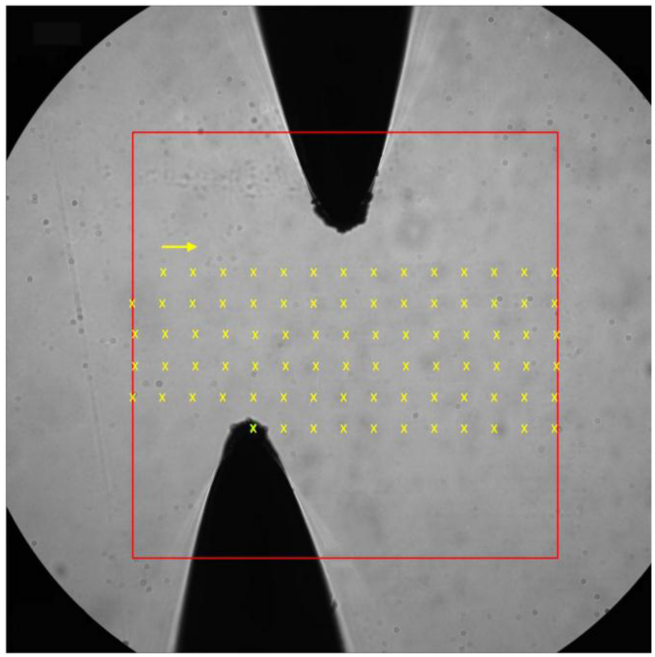

Fig. 5. Calibration procedure for identification of the transformation matrix between the needle and task spaces.

The particle position p is estimated using blob detection-based machine vision algorithms in image space, which is also used as the task space. A calibration procedure is designed to identify a transformation matrix between the task space and the needle spaces as illustrated in Fig. 5. The calibration runs once at the beginning of experiments. The tip of the needle is identified using template matching. Each needle scans the workspace with a pre-defined path and collects the data from needle space ${}^nN$ and task space ${}^tN$ to calculate the transformation matrix ${}^tH_n$:

$${}^tN = {}^tH_n * {}^nN \tag{12}$$

TABLE I
THE OBTAINED PARAMETERIZED MODELS

Model	a	b	R^2	RMSE
$a\delta^{-b}$	5.35×10^7	3.29	0.97	1.03
$a(\delta+b)^{-2}$	4.98×10^4	-37.79	0.96	1.1

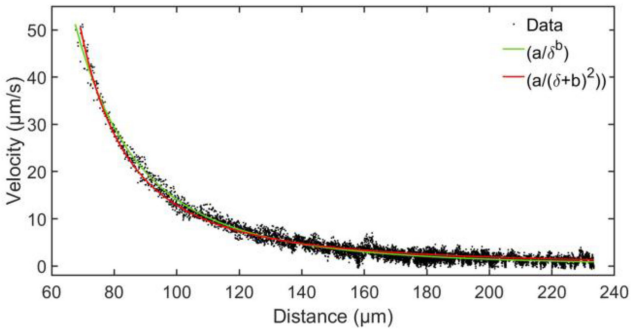

Fig. 6. Parameter estimation of velocity models from experimental data.

The obtained transformation matrix is then used for the experiments.

V. EXPERIMENTAL

A. Velocity Model

The theoretical velocity model of (9) can be written in the form of the parameterized model below:

$$\boldsymbol{v}_m\left(\delta_1, \delta_2\right) = a\left(\frac{1}{\left(\delta_1+b\right)^2}\boldsymbol{u}_1 + \frac{1}{\left(\delta_2+b\right)^2}\boldsymbol{u}_2\right) \tag{13}$$

where $a = C/(4\beta)^2$, $b = 1/(4\beta)$. $\boldsymbol{v}_m$ is the modeled velocity of the particle, corresponding to $\boldsymbol{v}_p$ in (9). Particle motion data from fifteen particles was collected using a constant voltage of 0.2 V and a corresponding current of 0.18A applied to the needle. The particle trajectories are recorded and the particle positions in each video frame was detected using the blob detection algorithm. Then, the velocities and the respective distances between the particle and the needle are calculated. The calculated velocity and distance data from all particles are combined for the parameter estimation of the model using non-linear least square method. The two needles are treated identical.

The identified velocity model for the needle is in the form of $a(\delta+b)^{-2}$ with R^2 of 0.96. However, we find that a more generic model $a\delta^{-b}$ gives a better fit, with R^2 of 0.97 as shown in Fig. 6 and Table I. Therefore, the following empirical model for $\boldsymbol{v}_m$ is used in the cooperative manipulation experiments:

$$\boldsymbol{v}_m\ \left(\delta_1, \delta_2\right) = a\left({\delta_1}^{-b}\boldsymbol{u}_1 + {\delta_2}^{-b}\boldsymbol{u}_2\right) \tag{14}$$

B. Cooperative Manipulation Experiments

The optimization-based control is implemented using Python 3.9.2. The vision feedback algorithms are implemented using OpenCV-Python 4.5.1.48. The optimization is realized using SciPy 1.7.0 Sequential Least-Squares Programming (SLSQP) method. The cooperation coefficient, $k_c = 0.5$ is used in the experiments.

TABLE II
THE OBTAINED MEAN ERROR, STANDARD DEVIATION, AND MAXIMUM ERROR FOR A DIFFERENT TYPE OF PATHS

Path type	Mean error (μm)	s.t.d. of error (μm)	Maximum error (μm)	Mean Velocity (μm/s)
Line	0.33	0.32	1.30	8.54
Square	0.77	0.55	2.32	8.39
Circle	0.89	0.66	2.82	8.65

The performance of the controller is validated using three experimental cases: line, square, and circle following. Each case was repeated five times and means and standard deviations of errors are calculated. Three of the repetitions are shown in Fig. 7. for clarity.

In the line following experiment, the particle was moved from left to right following a 125 μm line. In square paths following, the particle was started from the upper left corner of the square having a 125 μm side length. The diameter of the circular path is 100 μm. The obtained means and standard deviations of errors, and maximum error for different types of paths are summarized in Table II. The results show that the controller can have a line tracking accuracy better than 10% of the particle size, and for more demanding square and circle path following, the controller can achieve tracking better than 20% of the particle size.

The mean and maximum errors and standard deviations of errors increase from line to square to circle paths. For example, for the line path, the orientation of the line segment between the tips of the two needles N_1N_2 are little changed during the whole path when the needle positions change (see Movie 1). However, for the circle path following, both the positions of the needles and orientations of the line segment N_1N_2 change rather dramatically during the manipulation, leading to increased path tracking errors and uncertainty (see Movie 3). For the square path following, the dynamic of the needles is between the cases of line and circle path following (see Movie 2).

We also tested the cooperative manipulation system for more complex paths such as the infinity symbol and Aalto University logo paths, and the obtained results are shown in Fig. 8.

VI. CONCLUSION

In this paper, we reported a non-contact cooperative micromanipulation technique using two robotic electromagnetic needles. The motion of the microparticle is induced by a joint magnetic field gradient generated from the two needles. The trajectory of the particles is controlled by adjusting the positions of the needles using two 3 DOF nano-positioners. An optimization-based control was designed to achieve cooperation between two needles, to find the optimal needle positions that minimize the error between the modeled velocity and the target velocity, while avoiding potential collision of the needles.

The manipulator can precisely follow different given paths from a line to more complex letter-like paths. The experimental results show that the cooperative manipulator can achieve

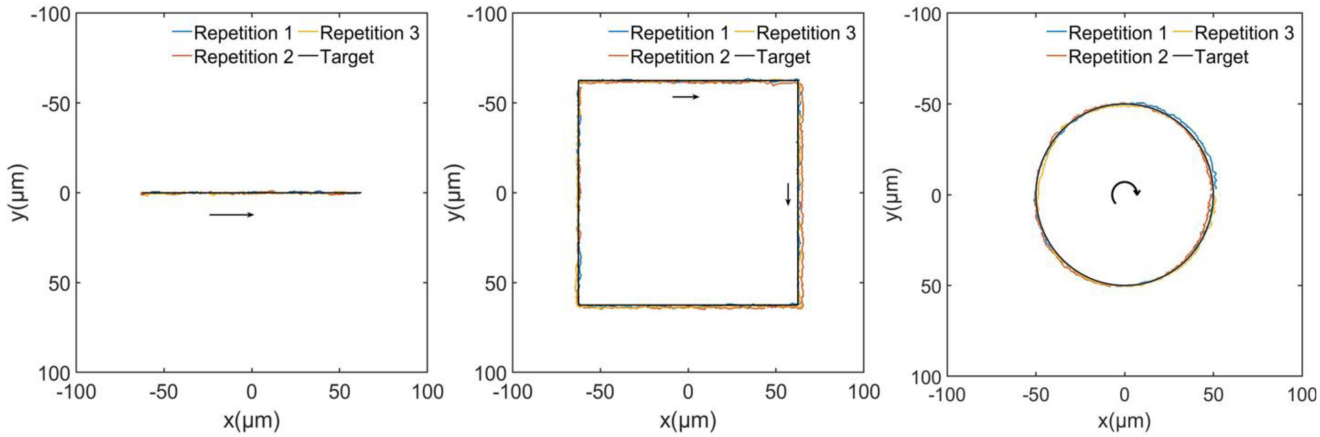

Fig. 7. Path following for 3 different paths (line, square, circle).

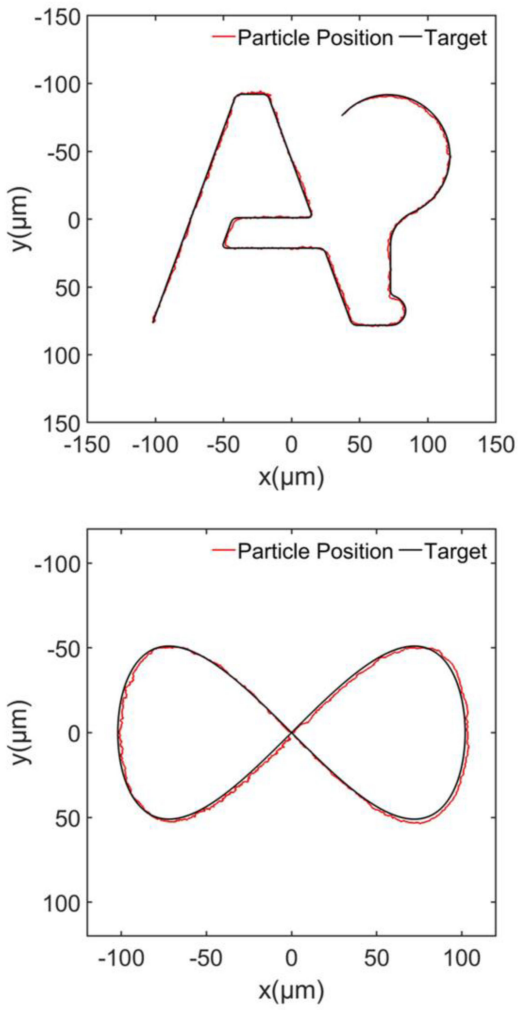

Fig. 8. Complex path following.

line following accuracy of $0.33 \pm 0.32\ \mu m$, square following accuracy of $0.77 \pm 0.55\ \mu m$ and circle following accuracy of $0.89 \pm 0.66\ \mu m$ μm with a 4.5 μm diameter superparamagnetic particle. The manipulator can also manipulate particles along complex paths such as the infinity symbol and the Aalto University logo.

The reported cooperative manipulation method will be integrated with the previous selective manipulation technology [13] for a particle-based in vitro drug delivery system for cell toxicology study. The method will also be extended with more needles and more accurate control of the magnetic field induced by the needle. In this work, only particle motion in *xy*-plane was considered, where *z*-axis motion will be address in our future work. Another aspect to be improved is the sampling frequency of the control system. The current frequency of about 10 Hz works reasonably for the experiments but may not be sufficient in applications. We will improve the efficiency of both the machine vision and optimization algorithms to achieve high sampling frequency to tackle possible high frequency disturbance to the particle from the environment including the Brownian motion.

ACKNOWLEDGMENT

The authors thank Dr. Zoran Cenev for the constructive discussion on the fabrication procedure of the electromagnetic needles, and Dr. Jean-Antoine Seon for the discussion during the design of the initial version of the control algorithms.

REFERENCES

[1] F. Caccavale and M. Uchiyama, "Cooperative manipulation," in *Springer Handbook of Robotics*. Springer International Publishing, 2016, pp. 989–1006.
[2] H. M. Do, T. Y. Choi, and J. H. Kyung, "Automation of cell production system for cellular phones using dual-arm robots," *Int. J. Adv. Manuf. Technol.*, vol. 83, no. 5–8, pp. 1349–1360, Mar. 2016.
[3] C. Smith *et al.*, "Dual arm manipulation—A survey," *Rob. Auton. Syst.*, vol. 60, no. 10, pp. 1340–1353, 2012.
[4] S. Yang, H. Wen, Y. Hu, and D. Jin, "Coordinated motion control of a dual-arm space robot for assembling modular parts," *Acta Astronaut.*, vol. 177, pp. 627–638, Dec. 2020.
[5] G. Li, S. Cai, and L. Xie, "Cooperative control of a dual-arm rehabilitation robot for upper limb physiotherapy and training," in *Proc. IEEE/ASME Int. Conf. Adv. Intell. Mechatronics*, AIM, vol. 2019, Jul. 2019, pp. 802–807.
[6] H. Fleischer *et al.*, "Application of a dual-arm robot in complex sample preparation and measurement processes," *J. Lab. Autom.*, vol. 21, no. 5, pp. 671–681, Oct. 2016.
[7] O. Felfoul *et al.*, "Magneto-aerotactic bacteria deliver drug-containing nanoliposomes to tumour hypoxic regions," *Nature Nanotechnol.*, vol. 11, no. 11, pp. 941–947, Nov. 2016.

[8] D. J. Cappelleri and Z. Fu, "Towards flexible, automated microassembly with caging micromanipulation," in *Proc. IEEE Int. Conf. Robot. Automat.*, pp. 1427–1432, 2013.
[9] J. J. Abbott, E. Diller, and A. J. Petruska, "Magnetic methods in robotics," *Annu. Rev. Control. Robot. Auton. Syst.*, vol. 3, no. 1, pp. 57–90, 2020.
[10] M. Salehizadeh and E. Diller, "Two-agent formation control of magnetic microrobots in two dimensions," *J. Micro-Bio Robot*, vol. 12, pp. 9–19, 2017.
[11] E. Diller, J. Giltinan, and M. Sitti, "Independent control of multiple magnetic microrobots in three dimensions," *Int. J. Rob. Res.*, vol. 32, no. 5, pp. 614–631, 2013.
[12] Z. Cenev *et al.*, "Manipulating superparamagnetic microparticles with an electromagnetic needle," *Adv. Mater. Technol.*, vol. 3, no. 1, pp. 1–9, 2018.
[13] J. A. Seon, Z. Cenev, and Q. Zhou, "Automatic non-contact extraction and independent manipulation of magnetic particles using electromagnetic needle," *IEEE/ASME Trans. Mechatronics*, vol. 4435, no. 2, pp. 931–41, Dec. 2019.
[14] J. Yu, B. Wang, X. Du, Q. Wang, and L. Zhang, "Ultra-extensible ribbon-like magnetic microswarm," *Nature Commun.*, vol. 9, no. 1, pp. 3260, Dec. 2018.
[15] H. Xie *et al.*, "Reconfigurable magnetic microrobot swarm: Multimode transformation, locomotion, and manipulation," *Sci. Robot.*, vol. 4, no. 28, pp. eaav8006, 2019.
[16] F. Qiu, S. Fujita, R. Mhanna, L. Zhang, B. R. Simona, and B. J. Nelson, "Magnetic helical microswimmers functionalized with lipoplexes for targeted gene delivery," *Adv. Funct. Mater.*, vol. 25, no. 11, pp. 1666–1671, 2015.
[17] W. Hu, G. Z. Lum, M. Mastrangeli, and M. Sitti, "Small-scale soft-bodied robot with multimodal locomotion," *Nature*, vol. 554, no. 7690, pp. 81–85, 2018.
[18] Z. Cenev *et al.*, "Ferrofluidic manipulator: Automatic manipulation of nonmagnetic microparticles at the air – ferrofluid interface," *IEEE/ASME Trans. Mechatronics*, vol. 26, no. 4, pp. 1–9, May 2021.
[19] M. Hoop *et al.*, "Mobile magnetic nanocatalysts for bioorthogonal targeted cancer therapy," *Adv. Funct. Mater.*, vol. 28, no. 25, pp. 1–8, 2018.
[20] X. Wang *et al.*, "3D printed enzymatically biodegradable soft helical microswimmers," *Adv. Funct. Mater.*, vol. 28, no. 45, pp. 1–8, 2018.
[21] X. Wang *et al.*, "Intracellular manipulation and measurement with multipole magnetic tweezers," *Sci. Robot.*, vol. 4, no. 28, Mar. 2019, Art. no. eaav6180.
[22] A. Menciassi, M. Quirini, and P. Dario, "Microrobotics for future gastrointestinal endoscopy," *Minim. Invasive Ther. Allied Technol.*, vol. 16, no. 2, pp. 91–100, 2007.
[23] B. J. Nelson, I. K. Kaliakatsos, and J. J. Abbott, "Microrobots for minimally invasive medicine.," *Annu. Rev. Biomed. Eng.*, vol. 12, pp. 55–85, 2010.
[24] F. Mushtaq *et al.*, "Highly efficient coaxial TiO_2-PtPd tubular nanomachines for photocatalytic water purification with multiple locomotion strategies," *Adv. Funct. Mater.*, vol. 26, no. 38, pp. 6995–7002, 2016.
[25] R. Bernasconi *et al.*, "Magnetically navigable 3D printed multifunctional microdevices for environmental applications," *Addit. Manuf.*, vol. 28, no. 4, pp. 127–135, 2019.
[26] F. Ongaro, S. Pane, S. Scheggi, and S. Misra, "Design of an electromagnetic setup for independent three-dimensional control of pairs of identical and nonidentical microrobots," *IEEE Trans. Robot.*, vol. 35, no. 1, pp. 174–183, Nov. 2019.
[27] H. H. See, S. C. B. Herath, Y. Du, H. Asada, and P. C. Y. Chen, "Localized manipulation of magnetic particles in an ensemble," *IEEE Access*, vol. 6, pp. 24075–24088, Apr. 2018.
[28] A. H. B. De Vries, B. E. Krenn, R. Van Driel, and J. S. Kanger, "Micro magnetic tweezers for nanomanipulation inside live cells," *Biophys. J.*, vol. 88, no. 3, pp. 2137–2144, 2005.
[29] Z. Cenev *et al.*, "Manipulating superparamagnetic microparticles with an electromagnetic needle," *Adv. Mater. Technol.*, vol. 3, no. 1, 2018.
[30] X. Geng, M. Li, Y. Liu, Y. Li, W. Zheng, and Z. Li, "Analytical tension-distribution computation for cable-driven parallel robots using hypersphere mapping algorithm," *Mech. Mach. Theory*, vol. 145, 2020, Art. no. 103692.